Journal of Chromatography Open 8 (2025) 100271

Contents lists available at ScienceDirect

Journal of Chromatography Open

journal homepage: www.elsevier.com/locate/jcoa

Full comprehensive ion-pair-mediated anion exchange chromatography × ion-pair reversed-phase liquid chromatography fingerprinting of digested messenger ribonucleic acid drug substances

Niklas Carstensen [a], Ryan Karongo [b], Anne Mengel [b], Michael Lämmerhofer [a,*]

[a] Institute of Pharmaceutical Sciences, Pharmaceutical (Bio-)Analysis, University of Tübingen, Auf der Morgenstelle 8, 72076 Tübingen, Germany
[b] Bayer AG, 13342 Berlin, Germany

ARTICLE INFO

Keywords:
Ion-pair mediated anion exchange chromatography
mRNA analysis
Oligonucleotide analysis
Two-dimensional LC
RNase T1 digest

ABSTRACT

The growing interest in messenger RNA (mRNA) based therapeutics has increased the need for analytical method development to meet the desired standards for quality control of these novel drugs. The identity of the mRNA drug substance is usually confirmed via indirect approaches such as Sanger sequencing or next generation sequencing (NGS), or more direct approaches such as LC-MS/MS after digestion with specific RNases. These conventional bottom-up MS methodologies, however, usually require several partial digests with various RNases to get sufficient sequence coverage. In the present study, a comprehensive two-dimensional liquid chromatography (LC × LC) platform is presented, utilizing ion-pair-mediated anion exchange chromatography in the first dimension and ion-pair reversed-phase liquid chromatography in the second dimension and evaluated using the convex hull model for orthogonality determination. This platform can be employed for the fingerprinting of RNase T1 digested mRNA, enabling the distinction between different mRNAs based on the fingerprint of a full digestion with a single RNase. It could also be used to confirm its identity or help with sequencing efforts, when combined with high-resolution MS.

1. Introduction

mRNA based drugs have recently emerged as a new treatment modality for a vast variety of diseases and as highly efficacious vaccines [1]. The global utilisation of mRNA vaccines during the course of the COVID-19 pandemic has had a significant impact on the acceleration of research and development in the field of mRNA drugs. Several of these drugs have now entered into later stages of clinical trials for the potential application as cancer treatments [2]. mRNA-based therapeutics also hold great potential for treatment of infectious, autoimmune or cardiovascular diseases [3]. Therapeutic mRNAs are constructed by the same structural features as physiological mRNAs. On the 5'-end, they are modified with a 5'-cap, e.g., a 7-methylguanosine (m7G) terminal nucleotide linked to the first base via a triphosphate bridge (Cap-0). Endogenous mRNAs usually have a Cap-0 structure which can be further modified by methylating the 2'-hydroxyl of the ribose of the first and second nucleotide (Cap-1 and Cap-2), respectively. The 5'-Cap structure is essential for stability, translation initiation and helps to avoid immune responses [4,5]. On the 3'-end, mRNAs are modified with a sequence of adenylate nucleotides termed the polyA-tail which is usually about 100-150 nucleotides long. The polyA-tail increases stability of the mRNA and is essential for translation initiation [4,6]. With therapeutic mRNA, however, there is also the possibility of cleaving the polyA-tail into two sections and connecting these with a short linker. This process has been demonstrated to result in enhanced translation efficiency and is used for the BioNTech Comirnaty® Vaccine [7–9]. Recently, also branched polyA-tails have been developed and have been shown to have a positive effect on the increase in translation capacity of mRNA drugs [10]. Moving inwards from the 3' and 5'-ends are the untranslated regions (UTRs) of the mRNA. Both UTRs regulate translation efficiency. The 5'-UTR facilitates interaction of the mRNA with the ribosome during translation initiation, but can also hinder this process when long GC-rich parts of the sequence are located in the 5'-UTR [11]. The 3'-UTR, on the other hand, mainly influences mRNA stability. In therapeutic mRNA, the UTRs need to be designed to enhance translation efficiency, so usually UTRs from very highly expressed human genes like α- or β-globin are used. α-globin, for example, has been used in the BioNTech Comirnaty® Vaccine BNT162b2 [8]. Central to all

* Corresponding author.
E-mail address: michael.laemmerhofer@uni-tuebingen.de (M. Lämmerhofer).

https://doi.org/10.1016/j.jcoa.2025.100271
Received 18 August 2025; Received in revised form 11 October 2025; Accepted 13 October 2025
Available online 15 October 2025

physiological and therapeutic mRNA is the open reading frame (ORF). This part of the sequence codes for the target protein so its effective design is essential for optimal therapeutic benefit of the mRNA drug. ORFs can be codon optimized to enhance translational efficiency by promoting synonymous codons that are frequently recognised by the most abundant cellular tRNAs. This, in turn, has been shown to improve translation rates and increase protein expression. Nevertheless, excessively accelerated rates of protein translation can impede the process of proper folding, ultimately resulting in the production of non-functional proteins. For this reason, it has been noted that increasing the GC content improves mRNA stability and translation efficiency [12,13].

To confirm mRNA sequence for quality control purposes liquid chromatography interfaced with high-resolution mass spectrometry (LC-HRMS) is usually used to characterize the drug substance [14]. This powerful new tool, however, usually comes with several disadvantages. For example, high sequence coverage can only be achieved by performing several digestions or partial digestions of the mRNA with RNases of different specificity to generate unique fragments that can be accurately matched to the original sequence [15]. The combination of sophisticated bioinformatic tools, expensive HRMS, and the need for complex sample preparation, coupled with a yet unresolved lack of analytical robustness, renders bottom-up LC-MS approaches for sequencing still demanding. Additionally, other approaches like next-generation sequencing (NGS), Sanger sequencing or nanopore sequencing often are difficult to automate, have high error rate for short and low abundant transcripts or need even more extensive and complex data analysis [16,17].

Ion-pair-Reversed Phase Liquid Chromatography (IPRP) is one of the most widely used chromatographic modes for the analysis of nucleic acids. It involves most often the use of alkylamines (e.g., Triethylamine, Dibutylamine, or Tributylamine) as counter-ions for ion-pair (IP) formation with the negatively charged phosphate backbone in combination with a co-ion like acetate to increase the hydrophobic interaction of the very hydrophilic nucleic acid with the RP stationary phase. Depending on the mobile phase and lipophilicity of the IP agent, it is adsorbed to the RP stationary phase leading to a dynamic ion-exchange process. The use of IPRP for the analysis of mRNA and oligonucleotides has been extensively researched and explored following the increase in popularity of these drugs [18,19]. Many IPRP methods are now recommended by the USP for the analysis of several different critical quality attributes of mRNA drug substances [20]. When coupled to mass spectrometry, IPRP also has significant advantages compared to other chromatographic modes because of its high separation power and good signal intensity. However, for this purpose expensive and environmentally hazardous fluorinated alcohols (e.g., hexafluoroisopropanol (HFIP)) are usually employed as slightly acidic co-ions to the amine-type ion-pair agent, instead of acetate which often leads to pronounced ion suppression [21]. In recent years, anion exchange chromatography has been widely used for the separation of nucleic acids [22–24]. It is also ideally suited to the purification of biopharmaceuticals due to its inherent non-denaturing properties leaving the intricate and sensitive structures of these molecules intact. Typical anion exchange chromatography can be operated both in salt gradient or pH gradient mode or in a fusion of both modes [22]. Usually, the optimal mode is heavily dependent on the analytes and the used stationary phase which can be separated into strong anion exchanger (SAX) typically using a permanently charged surface modification (e.g., quaternary ammonium derivatives) and weak anion exchangers (WAX) often using diethylaminoethyl (DEAE) groups that are charged depending on mobile phase pH [22–25]. pH gradient or salt mediated pH gradient mode is most often used for the separation of proteins or monoclonal antibodies, because it effectively enables separation depending on their isoelectric points, whereas salt gradient mode can also be applied for nucleic acids or mABs in general. However, for very large nucleic acids (e.g., mRNA), it is necessary to use very high salt concentrations for the elution of these analytes, due to their highly charged nature resulting from their phosphate backbone. Because of this, in recent years ion-pair mediated anion exchange (IPAX) emerged as a third mode to alleviate problems like low recovery and carry-over resulting from inherently high interaction of nucleic acids with anion exchange resins [26,27]. In IPAX, weak ion-pair cations (e.g., tetramethylammonium chloride (TMAC) or choline chloride) are used to form partially ion-paired analytes effectively decreasing the number of charges on polyelectrolyte analytes enabling better elution behaviour for large nucleic acids and a better separation of analytes depending on their size [28]. This mode has already been successfully used for the separation of adeno-associated virus capsids and, shows a lot of promise for extended use with nucleic acids [28,29].

In this study, the potential of two-dimensional LC in full comprehensive LC × LC mode with UV detection for quality control of mRNA digests, e.g., for batch-to-batch control, via sample fingerprinting analysis is evaluated. For this purpose and the optimization of the resolution of the mRNA fragments in the two-dimensional chromatographic space, the orthogonality of retention profiles between salt and ion-pair mediated AEX, respectively, and IPRP is assessed by the convex hull method. Also, the ion-pair agent in the second dimension (^{2}D) has been optimized and the resultant LC × LC method employed for profiling of mRNA digests of two distinct mRNAs. To our knowledge, it is the first report of LC × LC fingerprinting for mRNA digests.

2. Experimental

2.1. Materials

Tripropylamine (≥ 98 %), hexylamine (99 %), octylamine (99 %) and acetic acid (≥ 99.99 %), TRIS (≥ 99.8 %), tetramethylammonium-chloride (5 M), EMSURE® NaCl, EMSURE® hydrochloric acid (37 %) and nuclease-free water were purchased from Sigma-Aldrich (Merck, Munich, Germany). Gradient grade acetonitrile (ACN), MS-grade Ethanol and Isopropanol were purchased from Carl Roth (Karlsruhe, Germany). RNase T1 (1000 U/µl) was obtained from ThermoFisher Scientific. Analytical research grade water type I (18.2 MΩ) was obtained by treatment of deionized water with Elga PureLab Chorus Ultra purification system (Veolia waters, Celle, Germany). Mobile phase pH was always adjusted in the aqueous component of the mobile phase by the addition of acetic acid or 37 % hydrochloric acid and thoroughly mixed and degassed in an ultrasonic bath before use.

2.2. mRNA samples

Two different mRNA samples were used in this study. CleanCap® eGFP mRNA (enhanced green fluorescent protein) was obtained from TriLink® Biotechnologies as a base unmodified product mimicking a fully processed mature mRNA at a concentration of 1.0 mg/ml in 1 mM sodium citrate pH 6.4 and stored at -80°C. Comirnaty XBB 1.5 containing Raxtozinameran as drug substance was procured from a local pharmacy (Batch.No: HD9869). Pure Raxtozinameran was obtained by extracting the mRNA from the lipid nanoparticle (LNP) formulation by a modified version of the isopropanol precipitation method reported in [30]. For this purpose, the refrigerated drug product was 1:10 diluted with a solution of 60 mM ammonium acetate in 100 % isopropanol, vortexed thoroughly and centrifuged at 13,200 x g for 15 min at 4°C. The resulting supernatant was separated from the mRNA pellet, and the pellet was washed with 100 % isopropanol. After centrifuging again at 13,200 x g for 15 min at 4°C the supernatant was discarded and the pellet washed with 70 % ethanol in nuclease free water before the supernatant was carefully removed and the pellet dried at room temperature under a laminar airflow bench. The dried sample was diluted in nuclease free water for immediate analysis or in 1 mM sodium citrate buffer (pH 6.5) for storage at -80°C. Full digestion with RNase T1 was performed for all samples by diluting the sample stock solution 1:5 with nuclease free water, adding 2000 U of RNase T1 to the sample solution and digesting in a Thermocycler for 30 min at 37°C followed by a

Table 1
Chromatographic conditions for 1D optimization and ^{2}D.

1D-Screening	Method 1	Method 2	Method 3	Method 4
Mobile Phase A	25 mM TRIS-HCl; $^{w}_{w}p$H 7.6	25 mM TRIS-HCl, $^{w}_{w}p$H 7.0	25 mM TRIS-HCl, $^{w}_{w}p$H 7.0	25 mM TRIS-HCl, $^{w}_{w}p$H 7.0
Mobile Phase B	25 mM TRIS-HCl + 2 M TMAC $^{w}_{w}p$H 7.6	25 mM TRIS-HCl + 2 M TMAC, $^{w}_{w}p$H 7.0	25 mM TRIS-HCl + 2 M TMAC, $^{w}_{w}p$H 7.0	25 mM TRIS-HCl + 2 M NaCl, $^{w}_{w}p$H 7.0
1D Gradient	5 min 0 %B; 5-125 min 5-70 % B; equilibration for 15 min (0.2 ml/min)	5 min 0 % B; 5-125 min 5-70 % B; equilibration for 15 min (0.2 ml/min)	5 min 0 % B; 5-125 min 5-70 % B; equilibration for 15 min (0.2 ml/min)	5 min 0 %B; 5-125 min 5-70 % B; equilibration for 15 min (0.2 ml/min)
Temperature	40°C	40°C	20°C/40°C/60°C	20°C/40°C/60°C
Flow rate	0.05 ml/min	0.05 ml/min	0.05/0.1 mL/min	0.05/0.1 ml/min
Injection Volume	5 µL	5 µL	5 µL	5 µL
Detection	UV, 260 nm, 40 Hz	UV, 260 nm, 40 Hz	UV, 260 nm, 40 Hz	UV, 260 nm, 40 Hz
2D Conditions	100 mM OAA	100 mM HAA	100 mM TPAA	
Mobile Phase A	100 % H2O + 100 mM octylammonium acetate (OAA); $^{w}_{w}p$H 7.0	100 % H2O + 100 mM hexylammonium acetate (HAA); $^{w}_{w}p$H 7.0	100 % H2O + 100 mM tripropylammonium acetate (TPAA); $^{w}_{w}p$H 5.2	
Mobile Phase B	90 % ACN + 100 mM octylammonium acetate (OAA); $^{w}_{w}p$H 7.0	75 % ACN + 100 mM hexylammonium acetate (HAA); $^{w}_{w}p$H 7.0	75 % ACN + 100 mM tripropylammonium acetate (TPAA); $^{w}_{w}p$H 5.2	
2D Gradient	0-0.1 min 5 % B 0.1-0.8 min 5-95 % B 0.8-0.9 min 5 % B or 0-0.05 min 5 % B 0.05-0.4 min 5-95 % B 0.4 min to 0.45 min 5 % B	0-0.1 min 5 % B 0.1-0.8 min 5-95 % B 0.8-0.9 min 5 % B or 0-0.05 min 5 % B 0.05-0.4 min 5-95 % B 0.4 min to 0.45 min 5 % B	0-0.1 min 5 % B 0.1-0.8 min 5-95 % B 0.8-0.9 min 5 % B or 0-0.05 min 5 % B 0.05-0.4 min 5-95 % B 0.4 min to 0.45 min 5 % B	
Temperature	60°C			
Flow rate	2.5 ml/min			
Detection	UV, 260 nm, 160 Hz			
Loop filling	74 %			
Sampling	2.0 min - 125 min			

10-minute heating at 90°C.

2.3. Instrumentation and software

All liquid chromatography (LC) experiments were performed on HPLC systems from Agilent Technologies (Waldbronn, Germany). The ^{1}D consisted of a bio-inert quaternary pump (G5654A), an autosampler (G4226A), a thermostatted column compartment (G1316A), a variable wavelength detector (VWD) (G7114B) with a 2 µL flow cell and a pressure release kit (G4236-60010) between the VWD and the 2D interface. The ^{2}D consisted of a binary high-pressure gradient UHPLC pump (G4220A), a valve drive (G1170A) equipped with a 2-pos/8-port valve (G4236A) and two 60 µl loops, a thermostatted column compartment (G1316A) and a diode array detector (DAD, G4212A). The data acquisition rate for the VWD in the ^{1}D was set to 40 Hz and 160 Hz for the ^{2}D DAD for all full comprehensive 2D-LC measurements. These instrumental components were assembled into an LC × LC instrumental setup without flow splitting. The chromatographic data were processed with OpenLab CDS Data Analysis Version 2.8 (Build 2.208.0.1473) and OpenLab CDS 2D-LC Software (Build 1.2.65) from Agilent Technologies (Waldbronn, Germany).

Data visualization of 1D chromatograms was carried out using OriginPro 2022 (OriginLab, Northampton, Massachusetts, USA). Convex hull- and boxplots were generated using R.4.4.2 (R Core Team Vienna, Austria).

2.4. Liquid chromatographic conditions

The non-porous polymethacrylate-based strong anion exchange column YMC Accura BioPro IEX QF (50 × 2.1 mm, 3 µm) was used for 1D method development in this study. The column chemistry is a quaternary trimethylammonium strong anion exchanger (SAX). It was employed finally in the ^{1}D separation. For all LC × LC experiments a Waters BEH oligonucleotide C18 (20 × 2.1 mm, 1.7 µm, 300 Å) was used in the ^{2}D. Four 1D methods were tested for the first dimension. The ^{2}D gradient remained constant with two different modulation times (0.90 and 0.45 min) tested and the method for the second dimension was developed through the testing of three different ion-pairing reagents. All

Table 2
Calculated theoretical peak capacities according to Eq. 1 for ^{1}D optimization; eGFP mRNA digest used as sample; for chromatographic conditions see Table 1.

1D-Screening	Method 1	Method 3	Method 4
Mobile Phase A	25 mM TRIS-HCl in 100 % H_2O pH: 7.6	25 mM TRIS-HCl in 100 % H_2O pH: 7.0	25 mM TRIS-HCl in 100 % H_2O pH: 7.0
Mobile Phase B	25 mM TRIS-HCl, 2 M TMAC in 100 % H_2O pH: 7.6	25 mM TRIS-HCl, 2 M TMAC in 100 % H_2O pH: 7.0	25 mM TRIS-HCl, 2 M NaCl in 100 % H_2O pH: 7.0
Gradient	5 min 0 % B, 5 - 125 min 5 - 70 % B, equilibration for 15 min (0.2 mL/min)	5 min 0 % B, 5 - 125 min 5 - 70 % B, equilibration for 15 min (0.2 mL/min)	5 min 0 % B, 5 - 125 min 5 - 70 % B, equilibration for 15 min (0.2 mL/min)
Column Temperature: **20°C** Flow rate: **0.05 mL/min**	-	**128**	**137**
Column Temperature: **20°C** Flow rate: **0.1 mL/min**	-	**144**	**129**
Column Temperature: **40°C** Flow rate: **0.05 mL/min**	**145**	**134**	**101**
Column Temperature: **40°C** Flow rate: **0.1 mL/min**	**174**	**162**	**115**
Column Temperature: **60°C** Flow rate: **0.05 mL/min**	-	**120**	**95**
Column Temperature: **60°C** Flow rate: **0.1 mL/min**	-	**159**	**111**

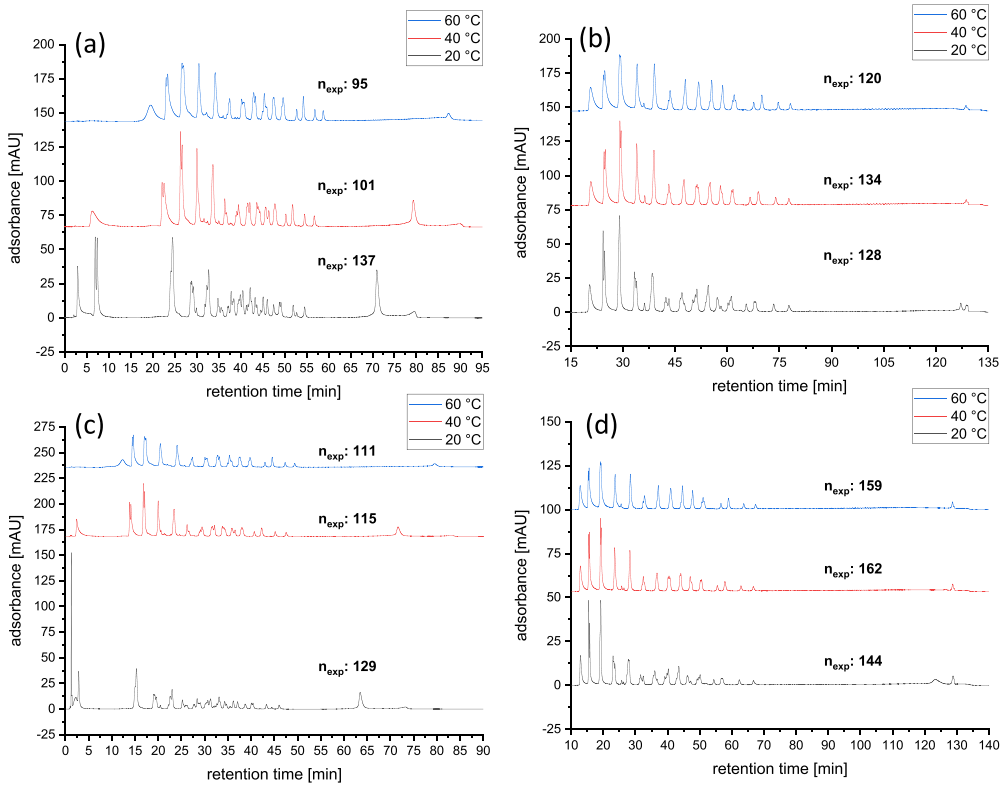

Fig. 1. [1]D optimization: Temperature study using method 3 with 2 M NaCl (a,c) and method 4 with 2 M TMAC (b,d) for elution with 0.05 (a,b) and 0.1 (c,d) ml/min flow rate. Other conditions see Table 1. Sample: CleanCap® eGFP mRNA digested with RNase T1.

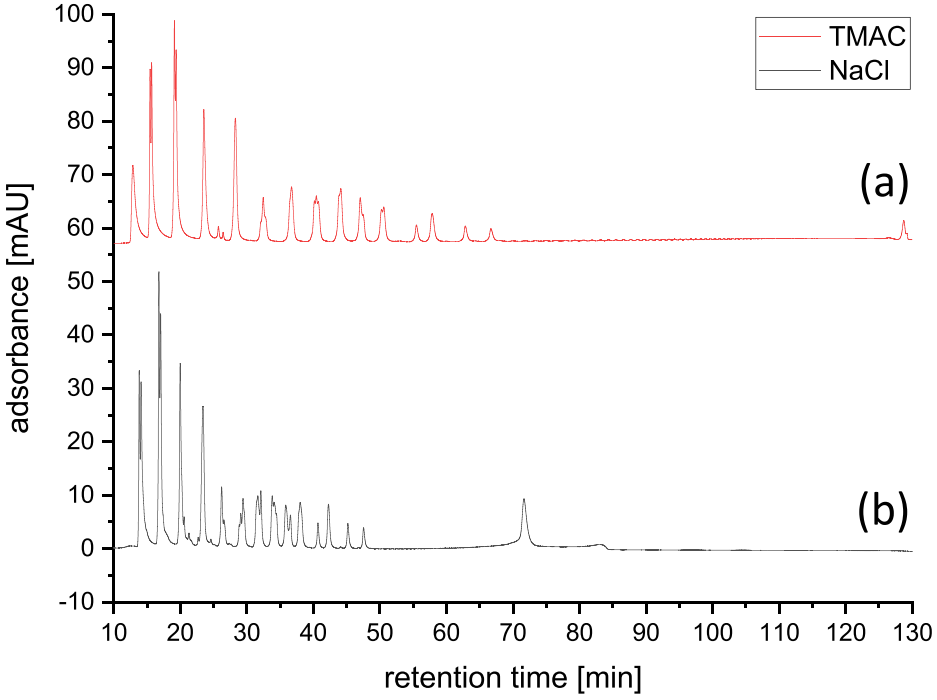

Fig. 2. Comparison of the retention behaviour for eGFP fragments when eluting with 2 M TMAC (a) or 2 M NaCl (b). Conditions: Temperature: 40°C; Flow rate: 0.100 mL/min; Sample: CleanCap® eGFP mRNA digested with RNase T1. Other conditions see Table 1.

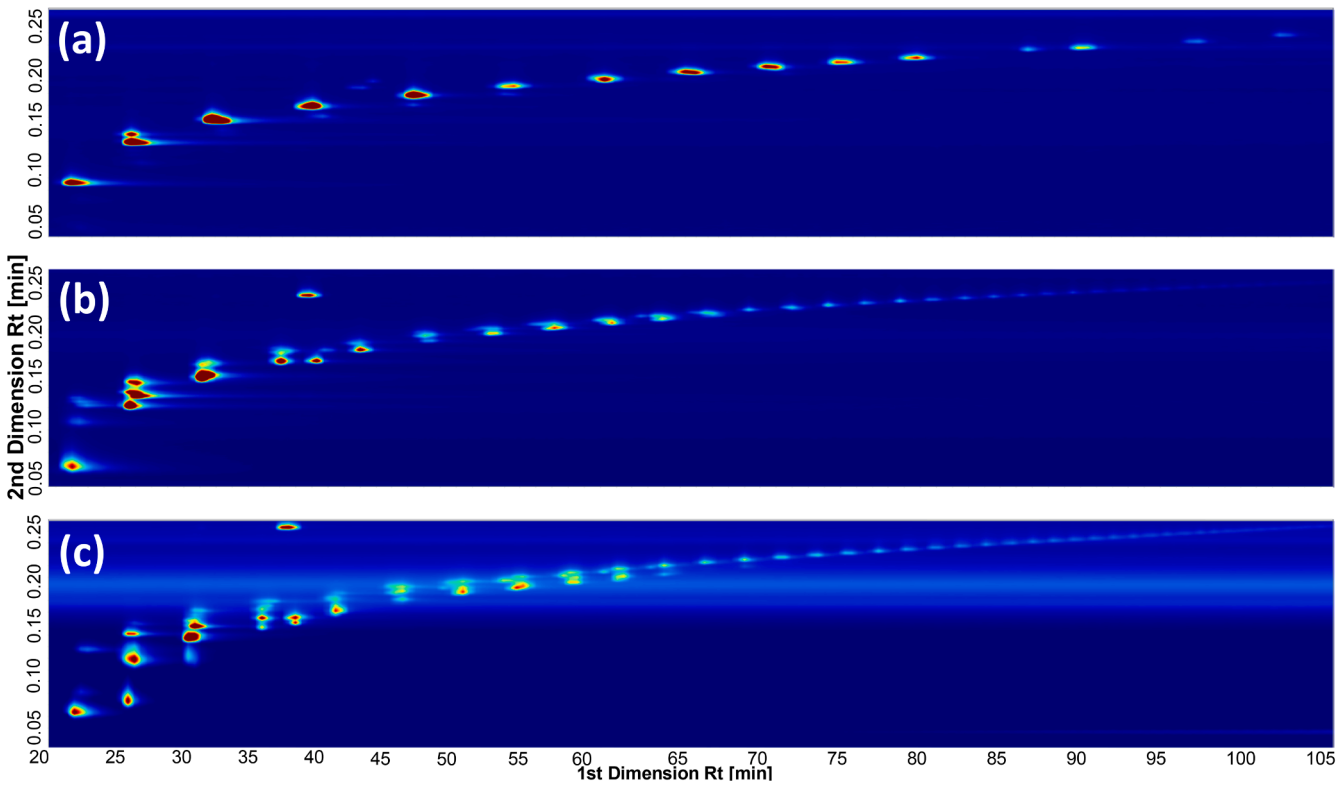

Fig. 3. Ion-pair reagent evaluation: Comparison of (a) 100 mM octylammonium acetate (OAA), (b) 100 mM hexylammonium acetate (HAA), and (c) 100 mM tripropylammonium acetate (TPAA). Other conditions, see Table 1, method 2.

gradients used for method development are shown in Table 1.

3. Results and discussion

3.1. ^{1}D method optimization

Since a direct comparison by chromatographic resolution is difficult for the analysis of complex sample mixtures like mRNA digests, the 1D screening results were evaluated based on the experimental peak capacity calculated by Eq. 1 [31,32],

$$\boldsymbol{n}(\boldsymbol{exp}) = 1 + \frac{\boldsymbol{t}(\boldsymbol{last}) - \boldsymbol{t}(\boldsymbol{first})}{1.7 \cdot \boldsymbol{w}(50\%)} \quad (1)$$

with *t(last)* and *t(first)* being the retention times of the first and last eluting fragments in the chromatogram, respectively, and *w(50 %)* the average peak width at 50 % peak height. The results of the screening are shown in Table 2 and the representative chromatograms in Fig. 1.

Preliminary experiments were conducted utilizing method 1 with a mobile phase of pH 7.6. This approach was later abandoned due to concerns that the ribose sugar of the mRNA would become unstable when exposed to slightly basic conditions for an extended period of time (during the long ^{1}D runs).. This instability could potentially result in misleading outcomes due to chemical alterations in the mRNA fragments generated by the digest that occur as the ribose undergoes hydrolysis. Because the autohydrolysis of the ribose is a spontaneous process encouraged by basic conditions the resulting chromatogram would probably show artefacts and reproducibility issues. For that reason, all subsequent analyses were performed at pH 7.0 to keep the fragments stable over the long ^{1}D runtime even though the peak capacities were slightly higher at pH 7.6 compared to pH 7.0. All calculated peak capacities are shown in Table 2. Analysis with TMAC regularly shows higher peak capacities than NaCl. This is because TMAC separates the fragments better by size, leading to stronger retention for the very large fragments in the digest (see Fig. 2). A reason for that could be that the interaction of the TMAC with the mRNA leads to disruption of its secondary structure and therefore to a linearization of the nucleic acid strand enabling more charged groups to interact with the stationary phase surface. TMAC also leads to the formation of large peak groups in contrast to narrower peaks when separating with NaCl. It has been demonstrated that this pronounced grouping of the peaks exerts a favorable influence on the two-dimensional separation. Consequently, TMAC emerges as the preferred option for the ^{1}D in comparison to NaCl, also due to slightly better compatibility with IPRP in ^{2}D.

In addition, the temperature has also been evaluated with experiments at 20°C, 40°C and 60°C. Digested mRNA fragments separated with NaCl exhibited a stronger retention with increasing temperature hinting at an endothermically driven interaction with the stationary phase. TMAC on the other hand exhibits an exothermic interaction process with the stationary phase because of slightly decreasing retention times with increasing temperatures. This temperature effect, however, is less strongly pronounced than with NaCl and probably results from compensating entropic and enthalpic contributions. TMAC shows higher retention time stability at changing temperature. Nevertheless, 40°C showed the highest peak capacity for TMAC at pH 7.0 and a flow rate of 0.1 mL/min (s.Fig.1d). This is in accordance with the already reported observations that the optimal temperature for a separation with TMAC seems to be between 30°C and 45°C [22].

3.2. Evaluation of ion-pairing reagents for the ^{2}D separation

For quality control purposes, IPRP is still the gold standard for nucleic acid analysis because of its good separation power regarding highly hydrophilic phosphorylated analytes like oligonucleotides or mRNA [33]. For LC-UV, the most commonly used alkylamine for ion-pairing is still triethylamine (TEA) in its acetate form (usually used at 100 mM in pure water or 25 % acetonitrile) [20]. TEA, however, is often not the most suitable choice as many other more hydrophobic

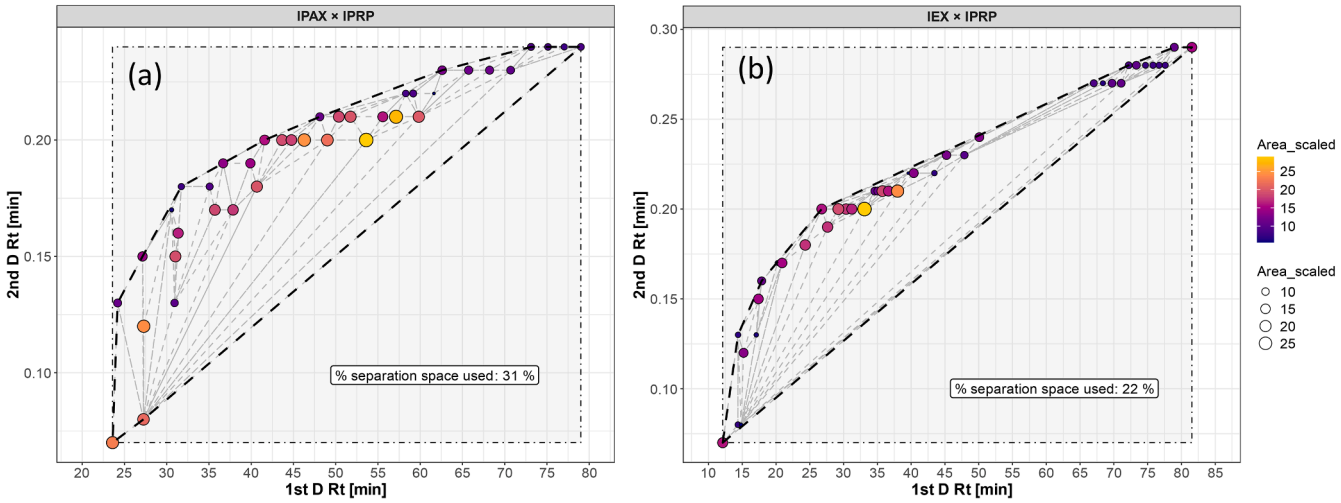

Fig. 4. Convex Hull orthogonality plots for (a) IPAX (with TMAC) × IPRP and (b) IEX (with NaCl) × IPRP experiments; peaks filtered by peak height to exclude background noise and potential instabilities in the baseline; lower boundary cutoff for TMAC: 110 and NaCl: 170. Conditions as specified in Table 1, method 3 (a) and method 4 (b).

alkylamines can lead to better resolution [34]. J. Maurer et al. for example evaluated different alkylamines based on their potential to separate large RNA molecules and came to the conclusion that moderately hydrophobic alkylamines like tripropylamine exhibited effective resolution of RNA fragments of 1500/2000 nucleotides in length whereas less hydrophobic ones like butylamine show superior separation of the larger fragments (4000/6000 nucleotides) [18]. However, the use of very strong ion-pairing reagents, such as tributylamine or dihexylamine, resulted in no effective separation. Their potential is presumably limited since they can only be used at lower concentrations (25 mM compared to 100 mM) and high amounts of ACN are necessary for their elution diminishing resolution. In this study, three IP agents were evaluated based on their separation power in the ^{2}D. Octylamine was selected as a strongly hydrophobic IP agent, while tripropylamine and hexylamine were selected as moderately hydrophobic IP agents on the basis of their previously demonstrated potential [18,35]. While IP-RPLC is commonly performed at pH 8 to 9 to limit adsorption at column hardware, a pH in the range 5 to 7 was selected in our study for better solubility of the IP agents. To limit adsorption, biocompatible hardware (column and capillaries) was used. All IP agent screenings were performed by two-dimensional LC experiments with method 2 in the first dimension and a ^{1}D flow rate of 0.1 ml/min. In the ^{2}D the modulation time was 0.45 min (gradient specified in Table 1) and the flow rate in the ^{2}D was always set to 2.5 ml/min. The results of the screening are shown in Fig. 3. Out of the three tested IP agents, octylamine showed the worst separation of the mRNA fragments (Fig. 3a) and tripropylamine exhibited the best (Fig. 3c) based on the number of peaks separated in the second dimension visible in the contour plots. Accordingly, further experiments were performed with tripropylamine as ion-pairing reagent.

3.3. LC × LC contour plot evaluation

To evaluate the surface coverage of separated compounds across the two-dimensional separation space, various orthogonality metrics have been developed to assess the effectiveness of 2D measurements [36]. Several of these orthogonality metrics like bin counting require the precise number of analytes in the sample mixture. Therefore, they are unsuitable to assess the LC × LC separation quality of complex mixtures like eGFP mRNA digests, where the number of resulting fragments is unknown, either due to proprietary untranslated regions (UTRs) or potential RNase T1 miscleavages leading to an incomplete sequence coverage [37]. Known parts of the eGFP sequence and the full Raxtozinameran sequence are shown in suppl. material S1 and S2. In this work, the convex hull model was chosen to evaluate orthogonality of the two used separation modes in the first (IPAX and IEX) and second (IPRP with tripropylamine) dimension. The convex hull was measured using Delauney triangulation as used in [38] with a custom R script. In computational geometry, the Delaunay triangulation of a set of points is defined as a unique triangulation in which a circle passing through the three apices of a triangle contains no other point [39]. The usable retention space was defined as a rectangle spanning the first and last eluting compound of the second and first dimension, respectively. The total percentage of used separation space was then calculated using Eq. 2.

$$\%\ separation\ space\ used = \left(\frac{Area_{convex\ \ hull}}{Area_{usable\ \ rete\ \ ntion\ \ space}}\right) \times\ 100 \qquad (2)$$

This parameter was then used as a comparable measure for orthogonality. The two convex hull plots corresponding to 2D-LC methods IPAX (with TMAC) × IPRP (method 3 in ^{1}D) and IEX (with NaCl) × IPRP (method 4 in ^{1}D) are depicted in Fig. 4 and have both been measured using TPAA as ion-pairing reagent in the second dimension with a modulation time of 0.45 min (see Table 1). The plots depict substance spots as peak area scaled by square root and show the scaled peak area as dots of different size and colour according to their scaled area. The surrounding usable separation space is given as a transparent grey rectangle underneath the convex hull with visible Delauney triangulation. To exclude peaks from background noise a peak height cutoff was implemented that is given for each convex hull in the caption. For the height cutoff the peak height scaled by its square root was used.

As evident from Fig. 4 the method using TMAC in the first dimension instead of NaCl leads to a better use of the separation space (31 % vs 22 %). This is surprising considering that TMAC adds another ion-pairing mechanism to the separation effectively increasing the similarity between the separation modes of the first and second dimension. However, TMAC is also known for separating nucleic acids better by size [29,40,41] leading to fragments of the digest being more grouped into clusters of similar size leading to better separation in the ^{2}D (compare Fig. 2) . In contrast, the better ^{1}D separation of method 4 (AEX with NaCl) cannot be further improved in the ^{2}D leading to less peak spread in the 2D-separation space. Furthermore, to evaluate the effect of undersampling on the separation, the undersampling correction factor was calculated according to Eq. 3 [42,43] that contains the second dimension cycle time $^{2}t_{c}$, the first dimension peak capacity $^{1}n_{c}$ that was already calculated according to Eq. 1 and the first dimension gradient time $^{1}t_{g}$. The

Table 3
Undersampling factor and effective peak capacities of relevant LC × LC experiments.

	Modulation time: 0.45 min ^{1}D flow rate: 0.05 ml/min	Modulation time: 0.90 min ^{1}D flow rate: 0.05 ml/min	Modulation time: 0.45 min ^{1}D flow rate: 0.1 ml/min
f_{cov}		0.31	
^2n_c	8	17	9
β	1.35	2.06	1.46
$n_{c,2D}$	252	350	309

resulting undersampling correction factor is then combined into the effective peak capacity (Eq. 4) [43] with the first and second dimension peak capacity ^1n_c and ^2n_c and a fractional coverage metric f_{cov} that reflects the orthogonality of the method calculated (31 %).

$$\textit{Undersampling correction factor } \beta = \sqrt{1 + 3.35\left[\frac{2_{t_c}\ 1_{n_c}}{1_{t_g}}\right]^2} \quad (3)$$

$$\textit{effective peak capacity } n_{c,2D}{}' = \frac{1_{nc} \times 2_{nc} \times f_{cov}}{\beta} \quad (4)$$

The resulting effective peak capacities are shown in Table 3.

Second dimension peak capacities are unsurprisingly highest with the modulation time of 0.9 min, but this also leads to the highest undersampling factor of 2.06. Essentially, the effective peak capacities are approximately the same for 0.05 ml/min as ^{1}D flow rate with 0.9 min modulation time and 0.1 ml/min as ^{1}D flow rate with 0.45 min modulation time with only a marginal difference. Obviously, this can be explained by the fact that the larger undersampling factor with longer modulation time can be overcompensated by the higher second dimension peak capacity which results from the longer gradient time and shallower gradient, respectively. This demonstrates that out of the tested methods an effective peak capacity optimized method was chosen.

3.4. Repeatability of the LC × LC fingerprints

To use the generated fingerprints for batch-to-batch quality control and to distinguish between different digested mRNAs, a confidence in

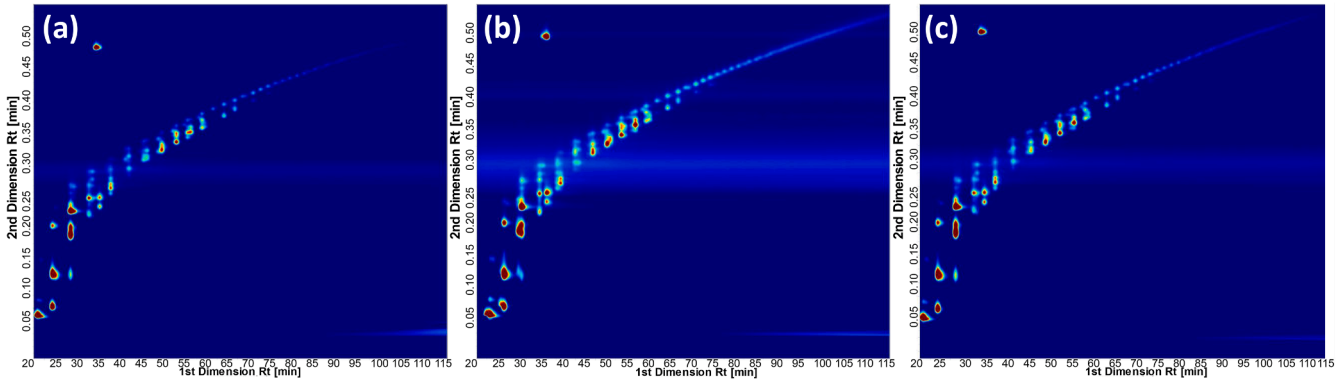

Fig. 5. Repeatability of LC × LC fingerprint of three different digests with RNase T1.

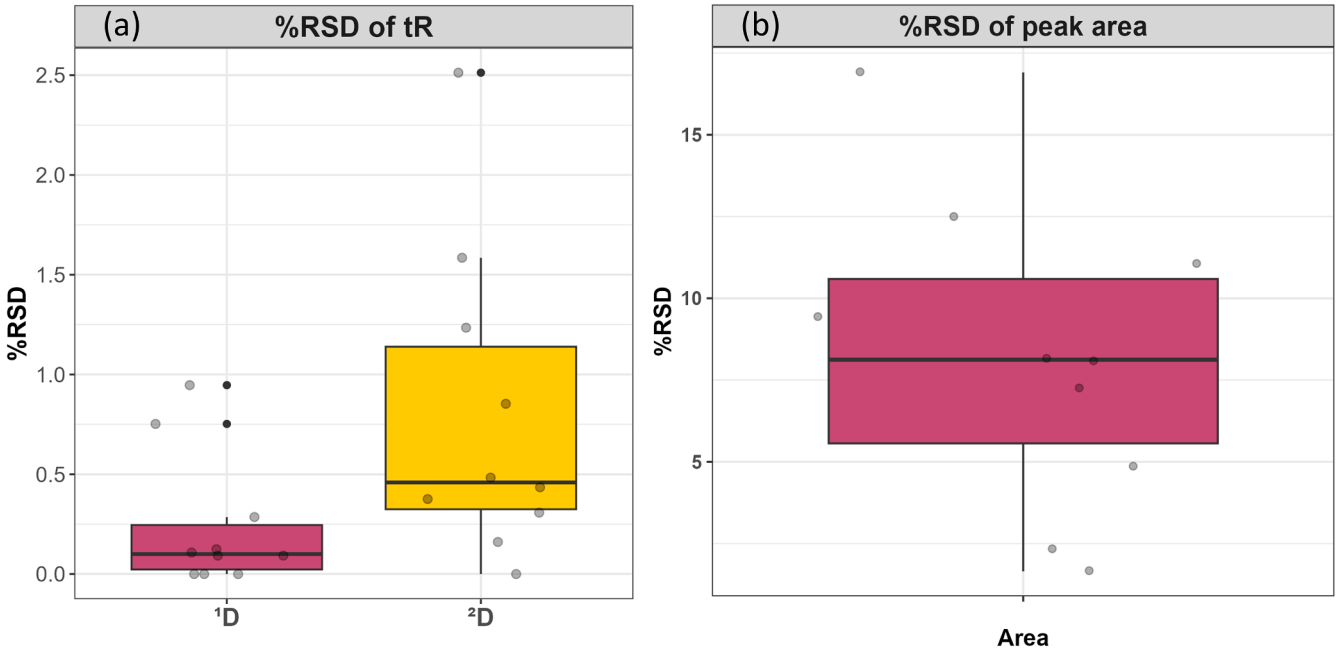

Fig 6. Box plot showing relative standard deviations (RSD [%]) for ^{1}D and ^{2}D retention times (a) and peak area (b) of the matched peaks in the contour plots of the three RNase T1 digests shown in Fig. 6. For selected peaks see suppl. Fig. S3.

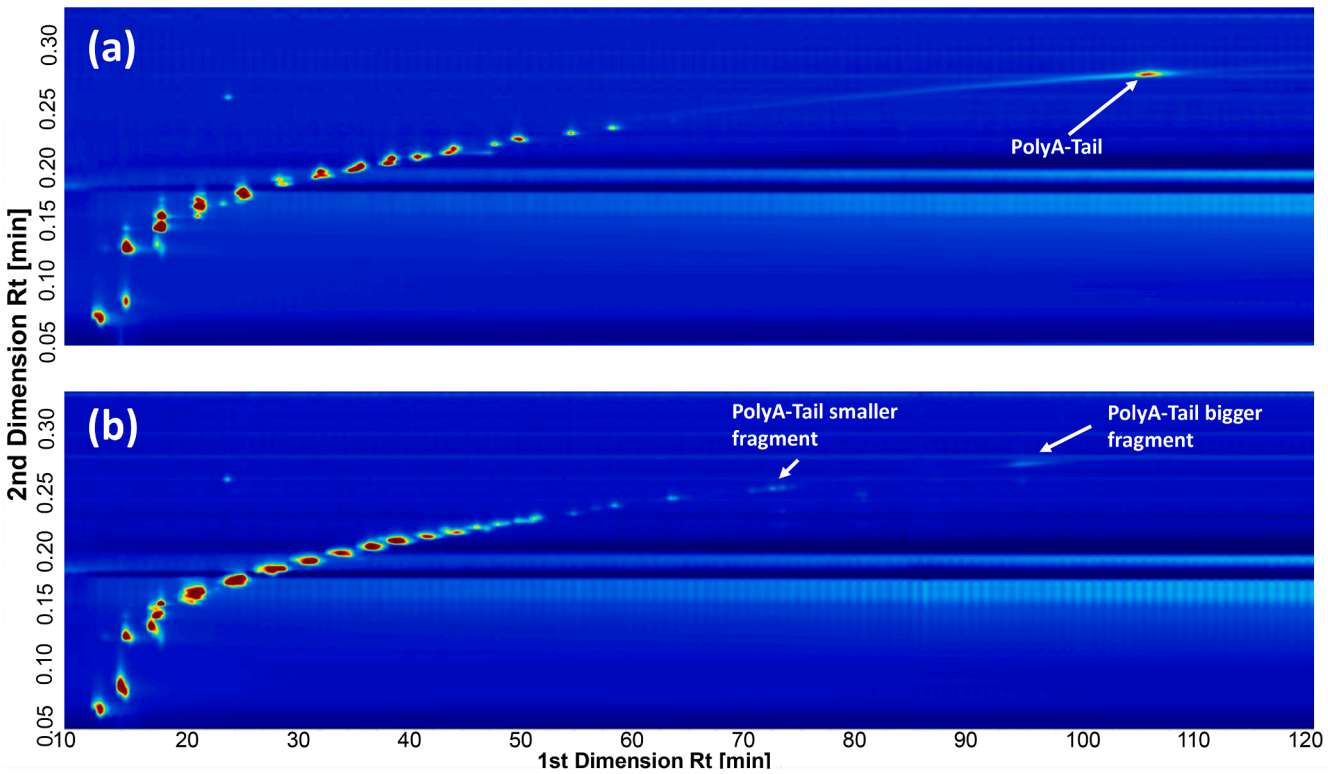

Fig. 7. Comparison of fingerprints of RNase T1 digests of (a) eGFP and (b) Vaccine (Raxtozinameran) mRNA. Conditions: flow rate: 0.1ml/min; Gradient: 5 min 0 % B, 5 - 125 min 5 - 80 % B, equilibration for 15 min at 0.2 mL/min.

their repeatability has to be established. For this purpose, the eGFP mRNA has been digested three times separately and each injected once per digestion. The digestion protocol is shown under 2.2. The resulting samples were analysed by AEX with TMAC in the ^{1}D (see Table 1; method 3) and the tripropylammonium acetate IPRP method in the ^{2}D using a modulation time of 0.9 min. The corresponding contour plots are shown in Fig. 5. Afterwards, each contour plot was adjusted in OpenLab CDS to the same contrast settings, and ten characteristic peaks were chosen, and their retention time and peak area repeatability were evaluated based on the relative standard deviation (RSD). The results are shown as boxplots in Fig. 6 (for selected peaks, their retention times and RSD [%] see suppl. material Fig. S3, S5 and S6). The fingerprints exhibit excellent retention time repeatability with the upper quartile below 0.25 % for the ^{1}D and only slightly above 1.0 % for the ^{2}D. Outliers exist for tested peaks of the ^{1}D but are below 1.0 % and for the ^{2}D ranging to 2.5 %. The relative standard deviation of the peak areas exhibits an upper quartile at about 10 %. The greater RSD for the peak areas can be attributed to non-biocompatible components of the systems, mainly the stainless steel autosampler. Overall, this proves that the fingerprints produced by the presented IPAX-LC × IPRP-LC setup exhibit adequate repeatability for QC and can be used to distinguish between different mRNA substances with sufficient confidence due to retention time stability.

3.5. *LC × LC fingerprints to distinguish between different mRNA digests*

To demonstrate the ability of the presented LC × LC setup to distinguish between digests of different mRNA substances, fingerprints were measured of eGFP and extracted Raxtozinameran using the optimized AEX method with TMAC in the ^{1}D dimension and a flow rate of 0.1 ml/min and the tripropylammonium acetate IPRP method in the ^{2}D with a modulation time of 0.45 min. The ^{1}D gradient was slightly adjusted to 80 % B instead of 70 % B to facilitate complete elution of the polyA-tail. The results are presented in Fig. 7. An overlay of the two contour plots shown in Fig. 7 is given in suppl. Fig.S4 so the shifts in retention for the peak groups are better visible. The most striking difference between the fingerprint of eGFP and Raxtozinameran is the long polyA-tail of the eGFP that is approximately 100-120 nucleotides (nt) in length according to previous mass spectrometric studies [44]. This is visible by the shooting star-like polyA-tail distribution that has its intensity maximum at about 108 min. The Raxtozinameran in contrast does not have a single long polyA-tail but is designed with a dual polyA-tail that is split into a 30 nt part and separated by a 10 nt linker (with two G residues as cleavage sites for RNase T1) from its long 70 nt counterpart (full sequence visible in S1). The peak visible in contour plot B at approximately 95 min most likely represents the 70 nt long part of the polyA-tail of Raxtozinameran. The distribution of the smaller fragment peaks across the contour plot differs also by retention time, resolution, and intensity indicating different fragments stemming from other digestion products relating to differences in length and sequence when comparing eGFP and Raxtozinameran. Overall, the differences in the contour plots demonstrates the substantial chromatographic selectivity of the presented IPAX-LC × IPRP-LC method for the smaller fragments across the contour plot and distinguishable larger characteristics structures like the polyA-tail distribution, which can be even more powerful when combined with mass spectrometric detection.

4. Conclusion

In this work, we developed a full comprehensive LC × LC platform with UV detection utilizing ion-pair mediated anion exchange chromatography in the first dimension coupled with ion-pair reversed phase chromatography in the second dimension to fingerprint complex mRNA digests. The first dimension was developed separately, and the optimized method was kept constant during the further optimization of the final LC × LC application for mRNA digests. IPAX was chosen over normal IEX in the first dimension because of a wider spread of the mRNA fragment peaks in the 2D-separation space and preferable 1D

performance. In fact, the combination of IPAX and IPRP exhibited better orthogonality (31 % vs. 22 %) compared to IEX with sodium chloride and IPRP setups. The orthogonality was tested with a convex hull approach using Delauneys triangulation which produces more accurate results for the convex hull according to Semard et al. [38]. In the end, this platform was successfully applied to differentiate between the different mRNAs of eGFP and Raxtozinameran from Comirnaty XBB 1.5. This demonstrates the direct applicability of this LC × LC fingerprinting setup to distinguish mRNA based in their full RNase T1 digests and offers further application in mRNA quality control through increases in fragment resolution when coupled to mass spectrometry for sequencing. For this purpose, further optimizations of the orthogonality seem to be warranted (e.g., testing HILIC instead of IPRP) and the MS compatibility of the ^{2}D has to be ascertained and improved, respectively.

CRediT authorship contribution statement

Niklas Carstensen: Writing – review & editing, Writing – original draft, Visualization, Methodology, Investigation, Formal analysis, Data curation, Conceptualization. **Ryan Karongo:** Writing – review & editing, Supervision, Resources, Conceptualization. **Anne Mengel:** Writing – review & editing, Methodology. **Michael Lämmerhofer:** Writing – review & editing, Supervision, Resources, Methodology, Funding acquisition, Conceptualization.

Declaration of competing interest

The authors declare the following financial interests/personal relationships which may be considered as potential competing interests:

The Author M. Laemmerhofer, given his role as Advisory Editorial Board member in J. Chromatography Open, had no involvement in the peer review of this article and had no access to information regarding its peer review. Full responsibility for the editorial process for this article was delegated to another journal editor.

Acknowledgements

Financial support of this research by Bayer AG, Berlin is gratefully acknowledged. We are also grateful to Agilent Technologies for support of this research by 2D-LC instrumentation through Agilent Research Awards (#4068 and 4610).We are grateful to YMC Europe, and Dr. Daniel Eßer and Dr. Feiyang Li for supporting this research with columns.

Supplementary materials

Supplementary material associated with this article can be found, in the online version, at doi:10.1016/j.jcoa.2025.100271.

Data availability

Data will be made available on request.

References

[1] K.S. Corbett, D.K. Edwards, S.R. Leist, O.M. Abiona, S. Boyoglu-Barnum, R. A. Gillespie, S. Himansu, A. Schafer, C.T. Ziwawo, A.T. DiPiazza, K.H. Dinnon, S. M. Elbashir, C.A. Shaw, A. Woods, E.J. Fritch, D.R. Martinez, K.W. Bock, M. Minai, B.M. Nagata, G.B. Hutchinson, K. Wu, C. Henry, K. Bahl, D. Garcia-Dominguez, L. Ma, I. Renzi, W.P. Kong, S.D. Schmidt, L. Wang, Y. Zhang, E. Phung, L.A. Chang, R.J. Loomis, N.E. Altaras, E. Narayanan, M. Metkar, V. Presnyak, C. Liu, M. K. Louder, W. Shi, K. Leung, E.S. Yang, A. West, K.L. Gully, L.J. Stevens, N. Wang, D. Wrapp, N.A. Doria-Rose, G. Stewart-Jones, H. Bennett, G.S. Alvarado, M. C. Nason, T.J. Ruckwardt, J.S. McLellan, M.R. Denison, J.D. Chappell, I.N. Moore, K.M. Morabito, J.R. Mascola, R.S. Baric, A. Carfi, B.S. Graham, SARS-CoV-2 mRNA vaccine design enabled by prototype pathogen preparedness, Nature 586 (2020) 567–571, https://doi.org/10.1038/s41586-020-2622-0.

[2] R. Yao, C. Xie, X. Xia, Recent progress in mRNA cancer vaccines, Hum. Vaccin Immunother. 20 (1) (2024) 2307187, https://doi.org/10.1080/21645515.2024.2307187.

[3] S. Qin, X. Tang, Y. Chen, K. Chen, N. Fan, W. Xiao, Q. Zheng, G. Li, Y. Teng, M. Wu, X. Song, mRNA-based therapeutics: powerful and versatile tools to combat diseases, Signal Transduct. Target. Ther. 7 (1) (2022) 166, https://doi.org/10.1038/s41392-022-01007-w.

[4] S.Khorshid Sokhangouy, M. Behzadi, S. Rezaei, M. Farjami, M. Haghshenas, Y. Sefidbakht, S. Mozaffari-Jovin, mRNA Vaccines: Design Principles, Mechanisms, and Manufacturing-Insights From COVID-19 as a Model for Combating Infectious Diseases, Biotechnol. J. 20 (2) (2025) e202400596, https://doi.org/10.1002/biot.202400596.

[5] S.C. Devarkar, C. Wang, M.T. Miller, A. Ramanathan, F. Jiang, A.G. Khan, S. S. Patel, J. Marcotrigiano, Structural basis for m7G recognition and 2′-O-methyl discrimination in capped RNAs by the innate immune receptor RIG-I, Proc. Natl. Acad. Sci. U. S. A. 113 (3) (2016) 596–601, https://doi.org/10.1073/pnas.1515152113.

[6] L. Jia, S.B. Qian, Therapeutic mRNA Engineering from Head to Tail, Acc. Chem. Res. 54 (23) (2021) 4272–4282, https://doi.org/10.1021/acs.accounts.1c00541.

[7] E. Fang, X. Liu, M. Li, Z. Zhang, L. Song, B. Zhu, X. Wu, J. Liu, D. Zhao, Y. Li, Advances in COVID-19 mRNA vaccine development, Signal Transduct. Target. Ther. 7 (1) (2022) 94, https://doi.org/10.1038/s41392-022-00950-y.

[8] X. Xia, Detailed Dissection and Critical Evaluation of the Pfizer/BioNTech and Moderna mRNA Vaccines, Vaccines (Basel) 9 (7) (2021) 734, https://doi.org/10.3390/vaccines9070734.

[9] Z. Trepotec, J. Geiger, C. Plank, M.K. Aneja, C. Rudolph, Segmented poly(A) tails significantly reduce recombination of plasmid DNA without affecting mRNA translation efficiency or half-life, RNA 25 (4) (2019) 507–518, https://doi.org/10.1261/rna.069286.118.

[10] H. Chen, D. Liu, J. Guo, A. Aditham, Y. Zhou, J. Tian, S. Luo, J. Ren, A. Hsu, J. Huang, F. Kostas, M. Wu, D.R. Liu, X. Wang, Branched chemically modified poly (A) tails enhance the translation capacity of mRNA, Nat. Biotechnol. 43 (2) (2025) 194–203, https://doi.org/10.1038/s41587-024-02174-7.

[11] K. Leppek, R. Das, M. Barna, Functional 5′ UTR mRNA structures in eukaryotic translation regulation and how to find them, Nat. Rev. Mol. Cell. Biol. 19 (3) (2018) 158–174, https://doi.org/10.1038/nrm.2017.103.

[12] A.A. Bicknell, D.W. Reid, M.C. Licata, A.K. Jones, Y.M. Cheng, M. Li, C.J. Hsiao, C. S. Pepin, M. Metkar, Y. Levdansky, B.R. Fritz, E.A. Andrianova, R. Jain, E. Valkov, C. Kohrer, M.J. Moore, Attenuating ribosome load improves protein output from mRNA by limiting translation-dependent mRNA decay, Cell. Rep. 43 (4) (2024) 114098, https://doi.org/10.1016/j.celrep.2024.114098.

[13] V.P. Mauro, S.A. Chappell, A critical analysis of codon optimization in human therapeutics, Trends Mol. Med. 20 (11) (2014) 604–613, https://doi.org/10.1016/j.molmed.2014.09.003.

[14] E.N. Welbourne, R.J. Copley, G.R. Owen, C.A. Evans, K. Isoko, K. Cook, J. Cordiner, Z. Kis, P.Z. Moghadam, M.J. Dickman, Mass spectrometry-based mRNA sequence mapping via complementary RNase digests and bespoke visualisation tools, Analyst 150 (5) (2025) 1012–1021, https://doi.org/10.1039/d5an00033e.

[15] A. Goyon, B. Scott, P. Yehl, K. Zhang, Online Nucleotide Mapping of mRNAs, Anal. Chem. 96 (21) (2024) 8674–8681, https://doi.org/10.1021/acs.analchem.4c00873.

[16] Y. Tu, A. Das, C. Redwood-Sawyerr, K.M. Polizzi, Capped or uncapped? Techniques to assess the quality of mRNA molecules, Curr. Opin. Syst. Biol. 37 (2024) 100503, https://doi.org/10.1016/j.coisb.2023.100503.

[17] X. Kang, A. Goyon, W. Stephenson, K. Zhang, Direct RNA modification mapping: Technological advances, gaps, and emerging trends, TrAC Trends Anal. Chem. 193 (2025) 5740–5749, https://doi.org/10.1016/j.trac.2025.118465.

[18] J. Maurer, C. Malburet, M. Francois-Heude, D. Guillarme, Evaluation of ion pairing reversed-phase liquid chromatography for the separation of large RNA molecules, J. Chromatogr. A 1740 (2025) 465574, https://doi.org/10.1016/j.chroma.2024.465574.

[19] M. Donegan, J.M. Nguyen, M. Gilar, Effect of ion-pairing reagent hydrophobicity on liquid chromatography and mass spectrometry analysis of oligonucleotides, J. Chromatogr. A 1666 (2022) 462860, https://doi.org/10.1016/j.chroma.2022.462860.

[20] Analytical Procedures for Quality of mRNA Vaccines and Therapeutics, 3rd Edition (2024), USP-NF; www.uspnf.com/notices/analytical-procedures-mrna-vaccines-20240802.

[21] B. Basiri, H. van Hattum, W.D. van Dongen, M.M. Murph, M.G. Bartlett, The Role of Fluorinated Alcohols as Mobile Phase Modifiers for LC-MS Analysis of Oligonucleotides, J. Am. Soc. Mass. Spectrom. 28 (1) (2017) 190–199, https://doi.org/10.1007/s13361-016-1500-3.

[22] M. Imiolek, S. Fekete, S. Rudaz, D. Guillarme, Ion exchange chromatography of biotherapeutics: Fundamental principles and advanced approaches, J. Chromatogr. A 1742 (2025) 465672, https://doi.org/10.1016/j.chroma.2025.465672.

[23] S.L. Khatwani, A. Pavlova, Z. Pirot, Anion-exchange HPLC assay for separation and quantification of empty and full capsids in multiple adeno-associated virus serotypes, Mol. Ther. Methods Clin. Dev. 21 (2021) 548–558, https://doi.org/10.1016/j.omtm.2021.04.003.

[24] C. Wagner, B. Innthaler, M. Lemmerer, R. Pletzenauer, R. Birner-Gruenberger, Biophysical Characterization of Adeno-Associated Virus Vectors Using Ion-Exchange Chromatography Coupled to Light Scattering Detectors, Int. J. Mol. Sci. 23 (21) (2022) 12715, https://doi.org/10.3390/ijms232112715.

[25] M.K. Aebischer, H. Gizardin-Fredon, H. Lardeux, D. Kochardt, C. Elger, M. Haindl, R. Ruppert, D. Guillarme, V. D'Atri, Anion-Exchange Chromatography at the Service of Gene Therapy: Baseline Separation of Full/Empty Adeno-Associated

Virus Capsids by Screening of Conditions and Step Gradient Elution Mode, Int. J. Mol. Sci. 23 (20) (2022) 12332, https://doi.org/10.3390/ijms232012332.
[26] S. Fekete, H. Yang, K. Wyndham, M. Lauber, Salt gradient and ion-pair mediated anion exchange of intact messenger ribonucleic acids, J. Chromatogr. Open 2 (2022) 100031, https://doi.org/10.1016/j.jcoa.2022.100031.
[27] S. Fekete, C. Doneanu, B. Addepalli, M. Gaye, J. Nguyen, B. Alden, R. Birdsall, D. Han, G. Isaac, M. Lauber, Challenges and emerging trends in liquid chromatography-based analyses of mRNA pharmaceuticals, J. Pharm. Biomed. Anal. 224 (2023) 115174, https://doi.org/10.1016/j.jpba.2022.115174.
[28] S. Kurth, T. Li, A. Hausker, W.E. Evans, R. Dabre, E. Muller, J. Kervinen, Separation of full and empty adeno-associated virus capsids by anion-exchange chromatography using choline-type salts, Anal. Biochem. 686 (2024) 115421, https://doi.org/10.1016/j.ab.2023.115421.
[29] S.M.K. Hua Yang, Weibin Chen, Anion-Exchange Chromatography for Determining Empty and Full Capsid Contents in Adeno-Associated Virus, Waters Application Note 720006825 (2020); www.waters.com/content/dam/waters/en/app-notes/2020/720006825/720006825-en.pdf.
[30] M. Packer, D. Gyawali, R. Yerabolu, J. Schariter, P. White, A novel mechanism for the loss of mRNA activity in lipid nanoparticle delivery systems, Nat. Commun. 12 (1) (2021) 6777, https://doi.org/10.1038/s41467-021-26926-0.
[31] U.D. Neue, Theory of peak capacity in gradient elution, J. Chromatogr. A 1079 (1-2) (2005) 153–161, https://doi.org/10.1016/j.chroma.2005.03.008.
[32] S. Chapel, M. Pardon, D. Cabooter, Systematic approach to online comprehensive 2D-LC method development for organic micropollutant profiling in wastewater, J. Chromatogr. A 1749 (2025) 465861, https://doi.org/10.1016/j.chroma.2025.465861.
[33] A.L.J. Webb, E.N. Welbourne, C.A. Evans, M.J. Dickman, Characterisation and analysis of mRNA critical quality attributes using liquid chromatography based methods, J. Chromatogr. A 1745 (2025) 465724, https://doi.org/10.1016/j.chroma.2025.465724.
[34] K.J.F. Martin Gilar, Yeva Budman, Uwe D. Neue, Kurt R. Yardley, Paul D. Rainville, Reb J. Russell II, John C. Gebler, Ion-pair reversed-phase high-performance liquid chromatography analysis of oligonucleotides: Retention prediction, J. Chromatogr. A 958 (2002) 167–182.
[35] S.M. McCarthy, M. Gilar, Hexylammonium Acetate as an Ion-Pairing Agent for IP-RP LC Analysis of Oligonucleotides, Waters Application Note 720003361 (2016).
[36] M. Gilar, P. Olivova, A.E. Daly, J.C. Gebler, Orthogonality of separation in two-dimensional liquid chromatography, Anal. Chem. 77 (2005) 6426–6434.
[37] M.R. Schure, J.M. Davis, Orthogonality measurements for multidimensional chromatography in three and higher dimensional separations, J. Chromatogr. A 1523 (2017) 148–161, https://doi.org/10.1016/j.chroma.2017.06.036.
[38] G. Semard, V. Peulon-Agasse, A. Bruchet, J.P. Bouillon, P. Cardinael, Convex hull: a new method to determine the separation space used and to optimize operating conditions for comprehensive two-dimensional gas chromatography, J. Chromatogr. A 1217 (33) (2010) 5449–5454, https://doi.org/10.1016/j.chroma.2010.06.048.
[39] D.T. Lee, A.K. Lin, Generalized Delaunay Triangulation for Planar Graphs,Discrete Comput, Geom 1 (1986) 201–217.
[40] H. Yang, S.M. Koza, W. Chen, Separation and Size Assessment of dsDNA Fragments by Anion-Exchange Chromatography (AEX), Waters Application Note 720007321 (2021).
[41] H. Yang, S.M. Koza, W. Chen, Plasmid Isoform Separation and Quantification by Anion-Exchange Chromatography (AEX), Waters Application Note 720007207 (2021).
[42] J.M. Davis, D.R. Stoll, P.W. Carr, Effect of First-Dimension Undersampling on Effective Peak Capacity in Comprehensive Two-Dimensional Separations, Anal Chem 80 (2008) 461–473.
[43] D.R. Stoll, P.W. Carr (Eds.), Multi-Dimensional Liquid Chromatography: Principles, Practice, and Applications, CRC Press, Boca Raton, 2022. https://doi.org/10.1201/9781003090557.
[44] J. Camperi, S. Lippold, L. Ayalew, B. Roper, S. Shao, E. Freund, A. Nissenbaum, C. Galan, Q. Cao, F. Yang, C. Yu, A. Guilbaud, Comprehensive Impurity Profiling of mRNA: Evaluating Current Technologies and Advanced Analytical Techniques, Anal. Chem. 96 (9) (2024) 3886–3897, https://doi.org/10.1021/acs.analchem.3c05539.